

Photoluminescence emission and Raman response of monolayer MoS₂, MoSe₂, and WSe₂

Philipp Tonndorf,¹ Robert Schmidt,¹ Philipp Böttger,¹ Xiao Zhang,¹ Janna Börner,² Andreas Liebig,¹ Manfred Albrecht,¹ Christian Kloc,³ Ovidiu Gordan,¹ Dietrich R. T. Zahn,¹ Steffen Michaelis de Vasconcellos,¹ and Rudolf Bratschitsch^{1,*}

¹Institute of Physics, Chemnitz University of Technology, 09107 Chemnitz, Germany

²Institute of Chemistry, Chemnitz University of Technology, 09107 Chemnitz, Germany

³School of Materials Science & Engineering, Nanyang Technological University, Singapore

*Rudolf.Bratschitsch@physik.tu-chemnitz.de

Abstract: We mechanically exfoliate mono- and few-layers of the transition metal dichalcogenides molybdenum disulfide, molybdenum diselenide, and tungsten diselenide. The exact number of layers is unambiguously determined by atomic force microscopy and high-resolution Raman spectroscopy. Strong photoluminescence emission is caused by the transition from an indirect band gap semiconductor of bulk material to a direct band gap semiconductor in atomically thin form.

©2013 Optical Society of America

OCIS codes: (160.6000) Semiconductor materials; (160.4236) Nanomaterials; (180.1790) Confocal microscopy; (180.5655) Raman microscopy; (300.6330) Spectroscopy, inelastic scattering including Raman; (300.6450) Spectroscopy, Raman; (300.6470) Spectroscopy, semiconductors; (300.6280) Spectroscopy, fluorescence and luminescence; (300.6250) Spectroscopy, condensed matter.

References and links

1. A. K. Geim, "Graphene: status and prospects," *Science* **324**(5934), 1530–1534 (2009).
2. K. S. Novoselov, D. Jiang, F. Schedin, T. J. Booth, V. V. Khotkevich, S. V. Morozov, and A. K. Geim, "Two-dimensional atomic crystals," *Proc. Natl. Acad. Sci. U.S.A.* **102**(30), 10451–10453 (2005).
3. V. Podzorov, M. E. Gershenson, C. Kloc, R. Zeis, and E. Bucher, "High-mobility field-effect transistors based on transition metal dichalcogenides," *Appl. Phys. Lett.* **84**(17), 3301–3304 (2004).
4. B. Radisavljevic, A. Radenovic, J. Brivio, V. Giacometti, and A. Kis, "Single-layer MoS₂ transistors," *Nat. Nanotechnol.* **6**(3), 147–150 (2011).
5. H. Fang, S. Chuang, T. C. Chang, K. Takei, T. Takahashi, and A. Javey, "High-performance single layered WSe₂ p-FETs with chemically doped contacts," *Nano Lett.* **12**(7), 3788–3792 (2012).
6. K. F. Mak, C. Lee, J. Hone, J. Shan, and T. F. Heinz, "Atomically thin MoS₂: a new direct-gap semiconductor," *Phys. Rev. Lett.* **105**(13), 136805 (2010).
7. A. Splendiani, L. Sun, Y. Zhang, T. Li, J. Kim, C. Y. Chim, G. Galli, and F. Wang, "Emerging photoluminescence in monolayer MoS₂," *Nano Lett.* **10**(4), 1271–1275 (2010).
8. Z. Yin, H. Li, H. Li, L. Jiang, Y. Shi, Y. Sun, G. Lu, Q. Zhang, X. Chen, and H. Zhang, "Single-layer MoS₂ phototransistors," *ACS Nano* **6**(1), 74–80 (2012).
9. H. S. Lee, S. W. Min, Y. G. Chang, M. K. Park, T. Nam, H. Kim, J. H. Kim, S. Ryu, and S. Im, "MoS₂ nanosheet phototransistors with thickness-modulated optical energy gap," *Nano Lett.* **12**(7), 3695–3700 (2012).
10. S. Tongay, J. Zhou, C. Ataca, K. Lo, T. S. Matthews, J. Li, J. C. Grossman, and J. Wu, "Thermally driven crossover from indirect toward direct bandgap in 2D semiconductors: MoSe₂ versus MoS₂," *Nano Lett.* **12**(11), 5576–5580 (2012).
11. H. Zeng, G.-B. Liu, J. Dai, Y. Yan, B. Zhu, R. He, L. Xie, S. Xu, X. Chen, W. Yao, and X. Cui, "Optical signature of symmetry variations and spin-valley coupling in atomically thin tungsten dichalcogenides," arXiv:1208.5864 (2012).
12. R. Späh, U. Elrod, M. Lux-Steiner, E. Bucher, and S. Wagner, "pn junctions in tungsten diselenide," *Appl. Phys. Lett.* **43**(1), 79–81 (1983).
13. R. Gordon, D. Yang, E. Crozier, D. Jiang, and R. Frindt, "Structures of exfoliated single layers of WS₂, MoS₂, and MoSe₂ in aqueous suspension," *Phys. Rev. B* **65**(12), 125407 (2002).
14. A. R. Beal, W. Y. Liang, and H. P. Hughes, "Kramers-Kronig analysis of the reflectivity spectra of 3R-WS₂ and 2H-WSe₂," *J. Phys. C*, **9**, 2449–2457 (1976).
15. A. Castellanos-Gómez, N. Agrait, and G. Rubio-Bollinger, "Optical identification of atomically thin dichalcogenide crystals," *Appl. Phys. Lett.* **96**(21), 213116 (2010).
16. M. M. Benameur, B. Radisavljevic, J. S. Héron, S. Sahoo, H. Berger, and A. Kis, "Visibility of dichalcogenide nanolayers," *Nanotechnology* **22**(12), 125706 (2011).

17. C. Lee, H. Yan, L. E. Brus, T. F. Heinz, J. Hone, and S. Ryu, "Anomalous lattice vibrations of single- and few-layer MoS₂," *ACS Nano* **4**(5), 2695–2700 (2010).
18. J. Verble and T. Wieting, "Lattice mode degeneracy in MoS₂ and other layer compounds," *Phys. Rev. Lett.* **25**(6), 362–365 (1970).
19. G. Frey, R. Tenne, M. Matthews, M. Dresselhaus, and G. Dresselhaus, "Raman and resonance Raman investigation of MoS₂ nanoparticles," *Phys. Rev. B* **60**(4), 2883–2892 (1999).
20. T. Wieting and J. Verble, "Infrared and Raman studies of long-wavelength optical phonons in hexagonal MoS₂," *Phys. Rev. B* **3**(12), 4286–4292 (1971).
21. C. Ataca, M. Topsakal, E. Aktürk, and S. Ciraci, "A comparative study of lattice dynamics of three- and two-dimensional MoS₂," *J. Phys. Chem. C* **115**(33), 16354–16361 (2011).
22. T. Korn, S. Heydrich, M. Hirmer, J. Schmutzler, and C. Schüller, "Low-temperature photocarrier dynamics in monolayer MoS₂," *Appl. Phys. Lett.* **99**(10), 102109 (2011).
23. H. Li, Q. Zhang, C. C. R. Yap, B. K. Tay, T. H. T. Edwin, A. Olivier, and D. Baillargeat, "From bulk to monolayer MoS₂: evolution of Raman scattering," *Adv. Funct. Mater.* **22**(7), 1385–1390 (2012).
24. A. Molina-Sánchez and L. Wirtz, "Phonons in single-layer and few-layer MoS₂ and WS₂," *Phys. Rev. B* **84**(15), 155413 (2011).
25. T. Sekine, M. Izumi, T. Nakashizu, K. Uchinokura, and E. Matsuura, "Raman scattering and infrared reflectance in 2H-MoSe₂," *J. Phys. Soc. Jpn.* **49**(3), 1069–1077 (1980).
26. T. J. Wieting, A. Grisel, and F. Levy, "Interlayer bonding and localized charge in MoSe₂ and α -MoTe₂," *Physica B+C* **99**(1-4), 337–342 (1980).
27. S. Sugai and T. Ueda, "High-pressure Raman spectroscopy in the layered materials 2H-MoS₂, 2H-MoSe₂, and 2H-MoTe₂," *Phys. Rev. B* **26**(12), 6554–6558 (1982).
28. Y. Ding, Y. Wang, J. Ni, L. Shi, S. Shi, and W. Tang, "First principles study of structural, vibrational and electronic properties of graphene-like MX₂ (M=Mo, Nb, W, Ta; X=S, Se, Te) monolayers," *Physica B* **406**(11), 2254–2260 (2011).
29. H. S. S. R. Matte, B. Plowman, R. Datta, and C. N. R. Rao, "Graphene analogues of layered metal selenides," *Dalton Trans.* **40**(40), 10322–10325 (2011).
30. D. G. Mead and J. C. Irwin, "Long wavelength optic phonons in WSe₂," *Can. J. Phys.* **55**(5), 379–382 (1977).
31. A. Kuc, N. Zibouche, and T. Heine, "Influence of quantum confinement on the electronic structure of the transition metal sulfide TS₂," *Phys. Rev. B* **83**(24), 245213 (2011).
32. R. Coehoorn, C. Haas, and R. de Groot, "Electronic structure of MoSe₂, MoS₂, and WSe₂. II. The nature of the optical band gaps," *Phys. Rev. B Condens. Matter* **35**(12), 6203–6206 (1987).
33. A. R. Beal and H. P. Hughes, "Kramers-Kronig analysis of the reflectivity spectra of 2H-MoS₂, 2H-MoSe₂ and 2H-MoTe₂," *J. Phys. Chem.* **12**, 881–890 (1979).
34. A. Anedda and E. Fortin, "Exciton spectra in MoSe₂," *J. Phys. Chem. Solids* **41**(8), 865–869 (1980).
35. J. Martin, N. Akerman, G. Ulbricht, T. Lohmann, J. H. Smet, K. von Klitzing, and A. Yacoby, "Observation of electron–hole puddles in graphene using a scanning single-electron transistor," *Nat. Phys.* **4**(2), 144–148 (2008).
36. Y. Ma, Y. Dai, M. Guo, C. Niu, J. Lu, and B. Huang, "Electronic and magnetic properties of perfect, vacancy-doped, and nonmetal adsorbed MoSe₂, MoTe₂ and WS₂ monolayers," *Phys. Chem. Chem. Phys.* **13**(34), 15546–15553 (2011).
37. W. S. Yun, S. Han, S. C. Hong, I. G. Kim, and J. Lee, "Thickness and strain effects on electronic structures of transition metal dichalcogenides: 2H-MX₂ semiconductors (M = Mo, W; X = S, Se, Te)," *Phys. Rev. B* **85**(3), 033305 (2012).
38. G. Plechinger, F. X. Schrettenbrunner, J. Eroms, D. Weiss, C. Schüller, and T. Korn, "Low-temperature photoluminescence of oxide-covered single-layer MoS₂," *Phys. Status Solidi (RRL)* **6**(3), 126–128 (2012).
39. M. P. Deshpande, G. K. Solanki, and M. K. Agarwal, "Optical band gap in tungsten diselenide single crystals intercalated by indium," *Mater. Lett.* **43**(1-2), 66–72 (2000).
40. J. A. Wilson and A. D. Yoffe, "The transition metal dichalcogenides discussion and interpretation of the observed optical, electrical and structural properties," *Adv. Phys.* **18**(73), 193–335 (1969).

1. Introduction

Graphene has been shown to be a prototypical two-dimensional material with exceptional physical properties [1]. However, the difficulty of creating an optical bandgap in graphene stimulated the search for other monolayer materials [2]. Layered transition metal dichalcogenides have attracted considerable attention due to their usability in fabricating electronic devices [3–5]. Monolayer MoS₂ has shown the surprising property of being photoluminescent [6,7], which renders this material also interesting for optical and optoelectronic [8,9] applications. Recently, photoluminescence of monolayer MoSe₂ [10] and WSe₂ [11] has been reported. Here, we investigate photoluminescence emission and absorption of MoS₂, MoSe₂, and WSe₂ monolayers and elucidate the nature of the layer-dependent phonon modes via high-resolution Raman spectroscopy.

2. Sample preparation and crystal structure

MoSe_2 and WSe_2 single crystals are grown by the vapor phase transport method [12]. As a reference, naturally grown MoS_2 is also investigated. Layered transition metal dichalcogenides of the form MX_2 ($M = \text{Mo}, \text{W}$ and $X = \text{Se}, \text{S}$) crystallize in a strongly covalently bound $X\text{-}M\text{-}X$ sandwich structure [13]. Consecutive $X\text{-}M\text{-}X$ layers are weakly bound by the van der Waals interaction. Layered transition metal dichalcogenides appear in different modifications, distinguished by their stacking orders. The $X\text{-}M\text{-}X$ layers of our investigated three material systems may crystallize as a hexagonal 2H structure belonging to the space group $P63/mmc$ (point group D_{6h}) with two MX_2 molecules inside the unit cell or as rhombohedral polytype 3R with three molecular layers per unit cell ($R3m$) [14]. Therefore, we perform X-ray diffraction measurements on suitably oriented single crystals of MoS_2 , MoSe_2 , and WSe_2 with a Seifert XRD 3000PTS diffractometer. For all samples we find a reflection unique to the 2H polytype (data not shown), i.e. all investigated materials belong to the 2H polytype. To obtain few- down to monolayer material the crystals are mechanically exfoliated [2] onto SiO_2/Si substrates. The number of layers is determined by optical interference and atomic force microscopy (AFM) measurements [15,16]. Figure 1 shows an optical micrograph, AFM image, and AFM line scan in contact mode of a flake of WSe_2 . Micron-sized regions of different heights in the range of nanometers are clearly identified. The AFM step height from a monolayer to the bilayer amounts to 0.7 nm (line scan in Fig. 1b), which is in excellent agreement with previous AFM studies (0.67 nm) [16]. The increased step height of 0.9 nm from the substrate to the monolayer material is attributed to adsorbates or other interactions between the monolayer and the substrate [17].

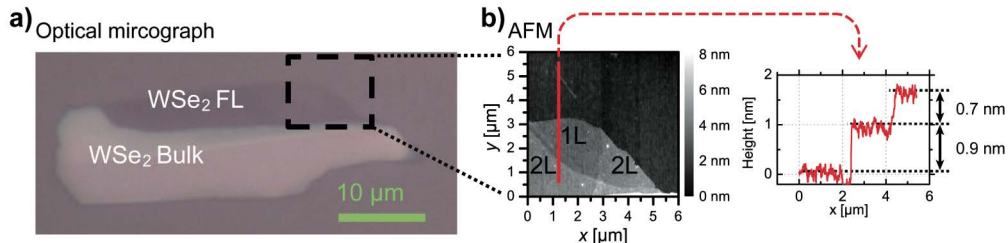


Fig. 1. Mechanically exfoliated WSe_2 on a SiO_2/Si wafer. (a) Optical micrograph under white light illumination. Few-layers (FL) appear purple next to the bright bulk WSe_2 . (b) Topography of marked area with height profile along red line, scanned with an atomic force microscope (AFM).

3. Raman spectroscopy

Raman spectroscopy has been shown to be a powerful tool to determine the exact number of layers of exfoliated MoS_2 . The energy, width, and amplitude of the vibrational modes are strongly influenced by the thickness of the flakes [17]. We investigate the vibrational modes of mono- and few-layer MoSe_2 and WSe_2 with high-resolution Raman spectroscopy. We use a Horiba LabRAM HR spectrometer with an excitation wavelength of 514.5 nm. The measurements are performed in a confocal micro configuration using a 100x microscope objective lens and a motorized xyz stage with 100 nm step size. Using a 2400 l/mm grating and a confocal pinhole of 100 μm the spectral resolution is below 1 cm^{-1} . The power of laser excitation measured below the microscope objective lens is 15 μW for MoS_2 and 68 μW for both MoSe_2 and WSe_2 . For bulk WSe_2 500 μW is used. All measurements are performed at room temperature. For simplicity we denote all vibrational modes with the irreducible representations of the D_{6h} point group of bulk material. A group-theoretical analysis predicts four Raman active modes for the D_{6h} group [18], i.e. three in-plane modes E_{1g} , E_{2g} , and E_{2g}^2 , and one out-of-plane mode A_{1g} (Fig. 2). In our experiment only E_{2g}^2 and A_{1g} are accessible. The E_{2g}^2 mode is at very low frequencies ($\sim 30 \text{ cm}^{-1}$), and the E_{1g} mode is forbidden in back-scattering geometry on a basal plane [19].

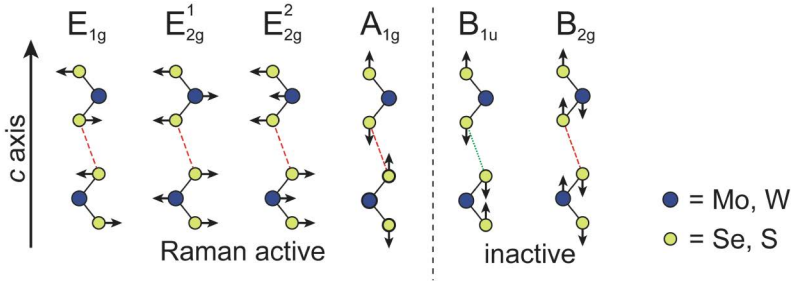


Fig. 2. Schematic drawing of the four Raman active and two inactive modes of the transition metal dichalcogenides MX_2 ($M = Mo, W$ and $X = Se, S$).

MoS_2

For bulk MoS_2 we observe both the in-plane $E^{1\text{g}}$ mode at 383.5 cm^{-1} and the out-of-plane $A_{1\text{g}}$ mode at 408.6 cm^{-1} (data not shown), in agreement with previous studies [17–23]. The separation between the two modes decreases with decreasing thickness of the material, which is an excellent indicator for the number of layers in MoS_2 [22–24].

$MoSe_2$

For bulk $MoSe_2$ the $A_{1\text{g}}$ mode shifts about 150 cm^{-1} towards lower wavenumbers compared to MoS_2 [25–27], which is also confirmed by calculations [28]. Indeed, we observe this out-of-plane mode in the spectral range of $240.5 - 242.5\text{ cm}^{-1}$, depending on the number of layers (Fig. 3).

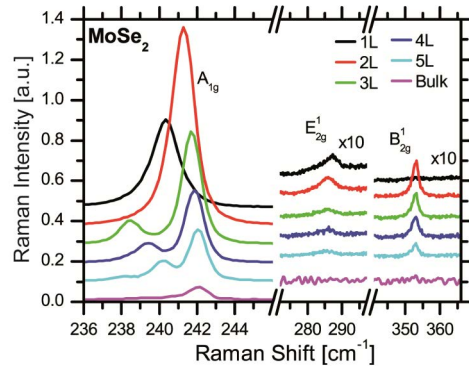


Fig. 3. Raman spectra of bulk and few-layer $MoSe_2$. Labels ‘1L’ – ‘5L’ indicate the number of layers. Raman spectra are vertically displaced for clarity.

As with MoS_2 , we find the characteristic softening of the mode (redshift) with decreasing thickness of the material. It amounts to 2 cm^{-1} from bulk to monolayer $MoSe_2$. Our measurements are in excellent agreement with two recent studies, where a Raman signal at 239.4 cm^{-1} on chemically exfoliated $MoSe_2$ with an unknown number of layers [29] and 243 cm^{-1} on a mechanically exfoliated $MoSe_2$ monolayer [10] were reported.

Our high experimental resolution allows us to observe a splitting of the out-of-plane Raman $A_{1\text{g}}$ line for the first time. Starting from one Raman line for mono- and bilayer $MoSe_2$ it splits into two for three and four layer material. For five layers of $MoSe_2$, three Raman lines appear. The spectral positions of the two maxima for three layers of $MoSe_2$ are arranged almost symmetrically with respect to the monolayer line. The range of the observed splittings is $2.4 - 3.2\text{ cm}^{-1}$. This effect is due to the so-called Davydov splitting, which appears due to the presence of more than one $MoSe_2$ molecule in the unit cell [18,24,25]. For the Raman

active A_{1g} mode the Se atoms in all layers oscillate in phase with respect to the corresponding center molybdenum atom, which does not move (Fig. 2, A_{1g}). The splitting occurs due to a varying number of phase shifts of 180° between the layers (Fig. 4). A phase shift of 180° between two layers is defined by the movement of the Se atoms: both top and bottom Se atoms within one layer move away from the molybdenum atom, while at the same time top and bottom Se atoms in the adjacent layer move towards the Mo atom and vice versa. Due to the weak interaction between the layers, the vibration frequencies of the in-phase and out-of-phase modes are almost degenerate [18]. However, each two adjacent layers vibrating in phase cause a small shift towards higher frequencies (indicated in Fig. 4 as a red dashed line), while two adjacent layers oscillating out of phase cause a shift towards lower frequencies by approximately the same amount (indicated in Fig. 4 as a green dotted line).

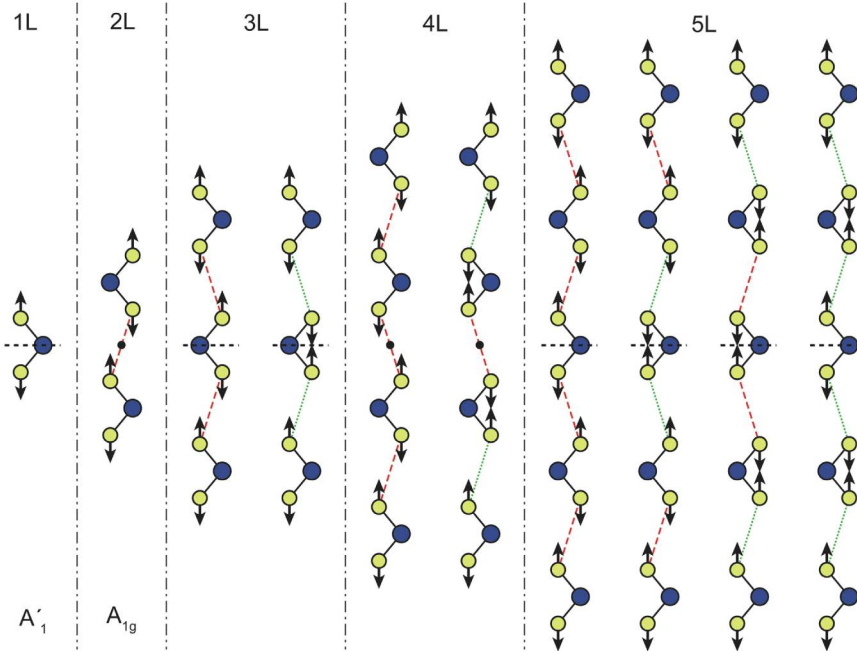


Fig. 4. Schematic drawing of all Raman active out-of-plane vibrational modes in 1 to 5 layers of MoSe_2 . Dashed red lines between the layers denote an increase of the mode frequency compared to non-interacting layers. Green dotted lines indicate a decrease of the oscillation frequency. The horizontal dashed line indicates the mirror plane σ_h of the unit cells with odd number of layers. The black dot marks the center of inversion for the unit cells with even number of layers. Due to a smaller unit cell, the out-of-plane mode for the monolayer is denoted A'_1 .

Obviously, for a monolayer only one Raman active out-of-plane mode (A'_1 , see Fig. 4) appears, since the unit cell contains only one MoSe_2 molecule and no translation symmetry along the c axis exists. For a bilayer with two MoSe_2 molecules per unit cell the situation is similar to bulk material with only one Raman active out-of-plane mode. However, the mode shifts towards higher wavenumbers compared to the monolayer due to the interlayer interaction. For few layer material with an odd number of layers only out-of-plane modes which preserve the symmetry elements of the monolayer A'_1 out-of-plane mode are Raman active. For our consideration, the most important symmetry element for these modes is the mirror plane σ_h indicated in Fig. 4. Therefore, for three layer material two Raman active out-of-plane modes are expected. For the first mode all layers are in phase, while for the second mode the center layer is 180° out of phase with respect to the two outer layers. The energies of these modes are arranged almost symmetrically to the monolayer mode, because the interlayer interactions induce an increase (decrease) of the energy for the first (second) mode.

For an even number of layers the out-of-plane modes with the same symmetry elements as the A_{1g} mode are Raman active. These modes exhibit an inversion center. Thus, for four layer material again two out-of-plane modes are Raman active. For the first mode all layers are in phase. For the second mode, the two outer layers are vibrating in opposite phase to the two inner layers. In five layer material one expects four different Raman active modes with none, one, two, and three layers being 180° out of phase with respect to the two outer layers. Two of these modes (with one and three inner layers vibrating out of phase) exhibit the same interlayer interaction and thus are degenerate. Indeed, we observe three maxima for the five layer material at 242.04 cm^{-1} , 240.12 cm^{-1} , and 238.03 cm^{-1} .

We now turn to the in-plane E_{2g}^1 mode, which appears at higher wavenumbers than A_{1g} in MoSe₂. In bulk MoSe₂ a weak vibrational mode was previously experimentally verified at 286 cm^{-1} [10,25–28]. Here, this mode is found at 287.2 cm^{-1} for monolayer and at 285.9 cm^{-1} for bilayer MoSe₂, indicating the same stiffening with decreasing numbers of layers as for MoS₂. Interestingly, at 353 cm^{-1} we observe a previously unknown Raman line for few-layer MoSe₂. The intensity of this mode is strongest for bilayer material and is reduced as the number of layers increases. Using similar considerations as above, we can assign this line to the B_{2g}^1 mode. This mode is inactive in bulk, but becomes Raman active due to the breakdown of translation symmetry in few layers. Besides these sharp lines ($\sim 1\text{ cm}^{-1}$), there are multiple broader maxima resulting from second order Raman processes (data not shown).

WSe₂

For bulk WSe₂, we find two distinct Raman signals at 248.0 and 250.8 cm^{-1} (Fig. 5). This doublet was also previously reported in a measurement of a WSe₂ crystal at a temperature of $T = 80\text{ K}$ [30]. The two lines are also in agreement with a recent calculation [28], predicting both the E_{2g}^1 and the A_{1g} mode to be close to 250 cm^{-1} .

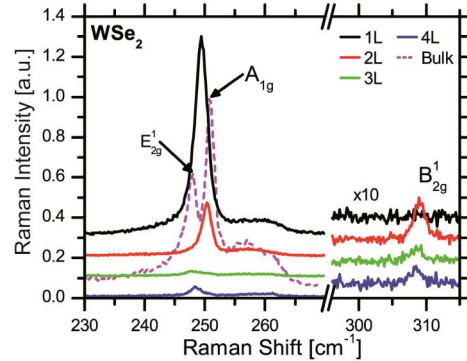


Fig. 5. Raman spectra of bulk and few-layer WSe₂. Labels ‘1L’ – ‘5L’ indicate the number of layers. Raman spectra are vertically displaced for clarity.

For few-layer WSe₂ we only find a single maximum, the position of which changes with the number of layers. Presently, it is not clear whether this single maximum is due to only one of the two lines, or the two modes are almost degenerate and cannot be resolved. Moreover, we also find a broad side maximum at 260 cm^{-1} and a small signature at 309 cm^{-1} for the bilayer. The latter can be assigned again to the normally inactive B_{2g}^1 mode [21,28]. As for MoSe₂, there are multiple broader maxima resulting from second order Raman processes (data not shown).

In summary, we find that Raman spectroscopy is an excellent tool to unambiguously pinpoint the number of sheets of the layered dichalcogenide materials MoSe₂ and WSe₂.

4. Photoluminescence emission

Recently, the transformation of MoS₂ from an indirect semiconductor in its bulk form to a direct semiconductor in case of a monolayer has been experimentally demonstrated [6,7]. As a consequence, substantial photoluminescence emission was detected. For bulk MoS₂, the fundamental indirect band gap originates from a transition from the top of the valence band at the Γ point to the bottom of the conduction band, which is about halfway between the Γ and K point. The direct band gap for bulk MoS₂ is higher in energy and occurs at the K point. The situation drastically changes, if the number of layers of MoS₂ is decreased. The energy of the fundamental indirect band gap increases, until it crosses the direct gap transition, which is virtually unchanged in energy [31]. In this way, monolayer MoS₂ becomes a direct band gap semiconductor and the photoluminescence intensity drastically increases with decreasing number of layers. We now compare the photoluminescence emission of MoSe₂, WSe₂, and MoS₂. A confocal microphotoluminescence setup is used to excite the sample with a continuous wave laser ($\lambda = 532$ nm), which is focused by a 100x microscope objective lens (NA = 0.9). Photoluminescence (PL) emission is collected by the same objective, dispersed with a $f = 150$ mm spectrometer and detected by a nitrogen cooled charge coupled device. All measurements are performed at room temperature.

MoSe₂

The energy of the indirect gap of bulk MoSe₂ is in the near-infrared [32] at 1.1 eV (1.13 μ m). The direct A and B excitons are higher in energy at 1.57 eV (790 nm) and 1.82 eV (682 nm) [33,34]. Figure 6a shows the photoluminescence spectrum of one, two, and three layers of exfoliated MoSe₂. The observed emissions from monolayer and bilayer MoSe₂ exhibit a single prominent maximum at 1.57 eV (792 nm) and 1.54 eV (807 nm), respectively.

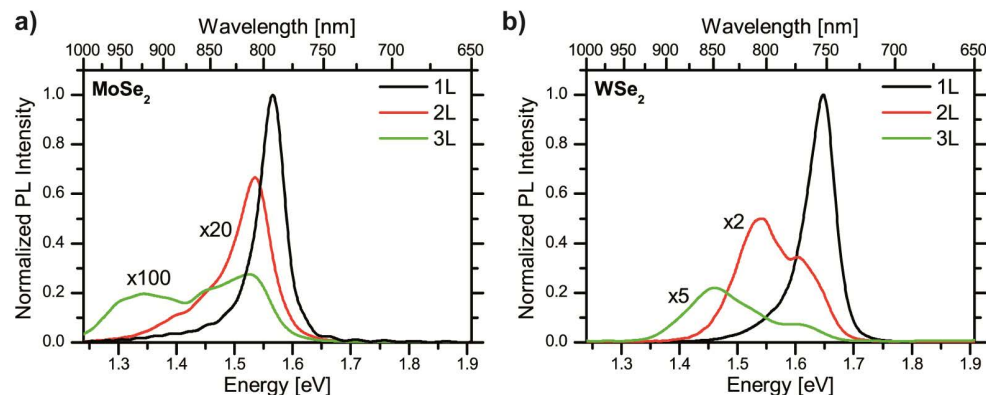


Fig. 6. Photoluminescence of monolayer and few-layer MoSe₂ (a) and WSe₂ (b). Spectra are recorded at room temperature, 532 nm excitation wavelength, and a fluence of 2100 W/cm² (a) and 250 W/cm² (b). PL spectra are Fourier-filtered with a 0.05 pixel⁻¹ short pass to remove etaloning due to the back-illuminated CCD camera.

Both emission lines are asymmetric with a steep edge at the high energy side and a broader tail at the low energy side. The peak positions vary slightly (± 5 nm) from sample to sample due to different environments caused by adsorbates or potential variations at the SiO₂ surface [35]. The PL intensities from the monolayer material are 10 - 20 times stronger than those of the bilayer material. The emission from the trilayer material shows two broad maxima at 1.53 and 1.35 eV (812 and 922 nm). The PL intensity decreases again by one order of magnitude as compared to the bilayer. The observed PL intensity maximum in photoluminescence for monolayer MoSe₂ is in excellent agreement with the known direct A exciton in the corresponding bulk material. This observation corroborates recent photoluminescence data of MoSe₂ [10] and model calculations [31,36,37] for other transition metal dichalcogenides, which show that the indirect gap increases in energy, while the direct

gap at the K point stays at about the same energy when decreasing the thickness from bulk to monolayer material. The valence band maximum and the conduction band minimum at the K point (direct gap) originate predominately from the strongly localized d orbitals at metal atom sites. Since the metal atoms are located in the middle of the X - M - X unit cell, there are only minimal interlayer interactions [6]. Therefore, the direct gap barely changes with decreasing layers. The observed decrease of PL intensity of MoSe_2 of one order of magnitude per additional layer is in accordance with measurements of MoS_2 [6]. The asymmetry of both monolayer emission maxima might be related to the presence of surface bound excitons as found for MoS_2 [38]. Already for bilayer MoSe_2 a direct band gap was predicted at the K point of the Brillouin zone [37], which could explain the single emission maximum of the measured photoluminescence. Only the MoSe_2 trilayer exhibits two well-separated maxima with one being at the same energy as for the bilayer (related to the A exciton) and the other assigned to the indirect band gap.

WSe_2

Bulk WSe_2 exhibits an indirect band gap in the near-infrared at 1.2 eV (1.03 μm). The direct A and B excitons have been reported in the range 1.4 - 1.8 eV (886 - 689 nm) [39] and at 2.30 eV (540 nm), respectively [40]. Figure 6b shows prominent photoluminescence of monolayer WSe_2 centered at 1.65 eV (752 nm). The emission has the same asymmetry as for MoSe_2 . Bilayer WSe_2 emits at 1.54 eV (806 nm) with a side maximum of 1.60 eV (773 nm). Interestingly, the PL intensity of the WSe_2 bilayer is only reduced by a factor of 4 compared to the monolayer. For a trilayer of WSe_2 , the side maximum nearly stays at the same position, while the main emission shifts towards a lower energy of 1.46 eV (849 nm). The smaller emission maxima of the bi- and trilayer again arise from the A exciton. The stronger maximum at the lower energy side is assigned to the indirect band gap, in agreement with previous studies on MoS_2 [6]. Our photoluminescence data are in excellent agreement with [11]. Differences in the relative intensities of the emission maxima might be related to the different excitation wavelength of 514 nm.

Photoluminescence emission vs. absorption of atomically thin MoS_2 , MoSe_2 , and WSe_2

To gain insight into the efficiency of the photoluminescence emission process we first investigate the role of absorption for each monolayer material. Due to multiple reflections at the interfaces of the $\text{MX}_2/\text{SiO}_2/\text{Si}$ structure, the absorption of laser light used for excitation is different as compared to a free-standing MX_2 monolayer. Since the Si substrate is non-transparent, one may use simple reflectivity measurements and the intensity of the Raman emission from the Si substrate at 528 nm, i.e. 520 cm^{-1} in the Raman signal, to extract the absorption of the MX_2 monolayers. A sketch of the optical system is given in Fig. 7. The absorption of the monolayer (neglecting scattering) is given by

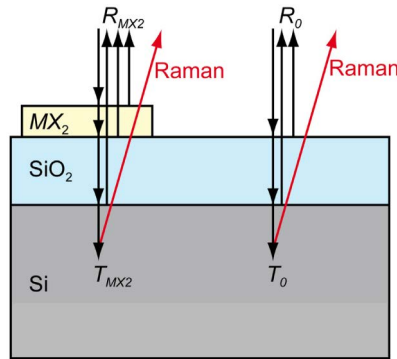


Fig. 7. Schematic drawing of reflected and transmitted light in the $\text{MX}_2/\text{SiO}_2/\text{Si}$ multilayer structure for the determination of the absorption in the MX_2 monolayer.

$$A_{MX_2} = R_0 - R_{MX_2} + T_0 - T_{MX_2},$$

where R_0 is the reflectivity of the bare SiO₂/Si substrate and R_{MX_2} is the reflectivity of the MX_2 /SiO₂/Si system, including all interferences. T_0 (T_{MX_2}) is the transmissivity into the thick Si wafer without (with) the monolayer on top. To eliminate calibration errors, we determine the ratio of reflected and transmitted light with and without the monolayer on top of the substrate:

$$r = I_{refl,MX_2} / I_{refl,substrate} = R_{MX_2} / R_0.$$

For the transmissivity ratio, we analyze the light entering the Si substrate. It is simply connected with the ratio of the Raman emission intensity from the Si substrate with and without the monolayer on top by

$$i_R = I_{Raman,MX_2} / I_{Raman,substrate} = (T_{MX_2} / T_0)^2.$$

We hereby assume that the absorption of the Raman laser with a wavelength of 514 nm, the Raman light from the substrate at 528 nm, and the exciting laser for the photoluminescence at 532 nm is about the same. The power of two originates from the fact that the Raman emission from the Si substrate is transmitted back through the same layered structure including multiple reflections before it reaches the detector (Fig. 7). After some algebra and the assumption that no light is absorbed in the SiO₂ layer, the absorption of the monolayers on a SiO₂/Si substrate is given by

$$A_{MX_2} = 1 - rR_0 - (1 - R_0)\sqrt{i_R}.$$

The retrieved values for A_{MX_2} are similar for the three monolayer materials deposited on SiO₂/Si substrate: $16 \pm 8\%$ (MoS₂), $23 \pm 8\%$ (MoSe₂), and $13 \pm 4\%$ (WSe₂). In contrast, the photoluminescence emission is always brightest for WSe₂ and faintest for naturally grown MoS₂, differing by at least an order of magnitude. This behavior might be indicative of a higher quantum yield of monolayer WSe₂. However, strong variations from flake to flake render a quantitative analysis difficult. Measurements on different substrates and free-standing layers are necessary to answer this question.

5. Conclusions

In conclusion, we have prepared monolayer and few-layer flakes of the transition metal dichalcogenides MoS₂, MoSe₂, and WSe₂. High-resolution Raman measurements show distinct layer dependent changes of the Raman signal including frequency shifts and splitting of the modes, which may be used to unambiguously identify the number of layers. We detect strong photoluminescence emission from monolayer MoSe₂ and WSe₂, indicative of direct gap semiconductors. These observations pave the way for optoelectronic devices based on these exceptional materials.

Acknowledgments

We thank Robert Magerle for granting access to the atomic force microscope and Mario Zerson for introducing us to its usage. We thank Andreas Zumbusch for providing an avalanche photodiode and Christian von Borczyskowski for a 100x microscope objective lens.